

Aurora Guard: Real-Time Face Anti-Spoofing via Light Reflection

Yao Liu[†] Ying Tai^{†*} Jilin Li[†] Shouhong Ding[†] Chengjie Wang[†] Feiyue Huang[†]

Dongyang Li[†] Wenshuai Qi[‡] Rongrong Ji[§]

[†]Youtu Lab, Tencent [‡]Shanghai University [§]Xiamen University

[†]{starimeliu, yingtai, jerolinli, ericshding, jasoncjwang, garyhuang, dongyangli}@tencent.com
[‡]qwspph@i.shu.edu.cn [§]rrji@xmu.edu.cn

Abstract

In this paper, we propose a light reflection based face anti-spoofing method named Aurora Guard (AG), which is fast, simple yet effective that has already been deployed in real-world systems serving for millions of users. Specifically, our method first extracts the normal cues via light reflection analysis, and then uses an end-to-end trainable multi-task Convolutional Neural Network (CNN) to not only recover subjects' depth maps to assist liveness classification, but also provide the light CAPTCHA checking mechanism in the regression branch to further improve the system reliability. Moreover, we further collect a large-scale dataset containing 12,000 live and spoofing samples, which covers abundant imaging qualities and Presentation Attack Instruments (PAI). Extensive experiments on both public and our datasets demonstrate the superiority of our proposed method over the state of the arts.

1 Introduction

Face anti-spoofing is currently a promising topic in computer vision research community, and also a very challenging problem in remote scenarios without specific hardware equipped in industry. The existing methods Liu *et al.* [2018]; Xie *et al.* [2017]; Yi *et al.* [2014] on face anti-spoofing are paying more attention on multi-modality information (*e.g.*, depth or infrared light). With the development of depth sensors, recent methods and commercial systems exploit hardwares that can be embedded with structured light (*e.g.*, FaceID on iPhone X), light field Xie *et al.* [2017] or LIDAR to reconstruct accurate 3D shape, which can well address the limitation of 2D methods towards high-level security Li *et al.* [2016, 2017]. Although these methods can achieve good classification performance, they highly rely on the customized hardware design, which unavoidably increases the system cost.

As a replacement, recent advances on Presentation Attack Detection (PAD) tend to estimate depth directly from a single RGB image. In particular, since 3D reconstruction from a single image is a highly under-constrained task due to the lack of strong prior of object shapes, such methods introduce certain

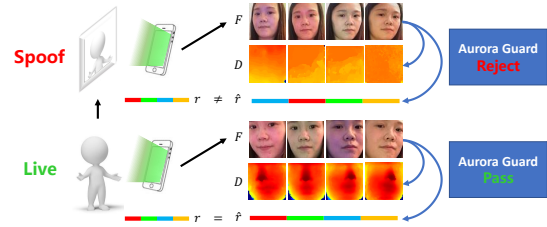


Figure 1: Framework of our proposed method. F_r denotes the facial reflection frame. D denotes the recovered depth map from solid depth clue, which improves our anti-spoofing performance against unlimited 2D spoofing. r denotes the light CAPTCHA generated and casted by light source, and \hat{r} is estimated by our method.

prior by recovering sparse Wang *et al.* [2013] or dense Atoum *et al.* [2017]; Liu *et al.* [2018] depth features. However, these methods still suffer from missing the solid depth clue. As a result, the corresponding liveness classifiers are hard to generalize to real presentation attacks in the wild.

Towards high accuracy and security without using depth sensors, we propose a simple, fast yet effective face anti-spoofing method termed Aurora Guard (AG). Its principle is to use light reflection to impose two auxiliary information, *i.e.*, the depth map and light parameter sequence, to improve the accuracy and security of PAD respectively (as shown in Fig. 1). In this paper, we propose and define the light parameters sequence as *light CAPTCHA*. By only incorporating a single extra light source to generate the reflection frames, our method holds the *efficiency* and *portability* of cost-free software methods, which has already been deployed on smart phones and embedded terminals that serves for *millions of users*.

More specifically, our method mainly consists of two parts: (1) Based on Lambertian model, we cast dynamic changing light specified by the random light CAPTCHA, and then extract the normal cues from facial reflection frames. (2) We use an end-to-end trainable multi-task CNN to conduct liveness classification and light CAPTCHA regression simultaneously. The classification branch estimates the depth maps from the normal cues, and classify liveness from the recovered depth map via a compact encoder-decoder structure. The regression branch estimates the light parameter sequence, which forms a light CAPTCHA checking mechanism to handle one special type of attack named *modality spoofing*, which is a very common attack in real scenarios.

* Corresponding author

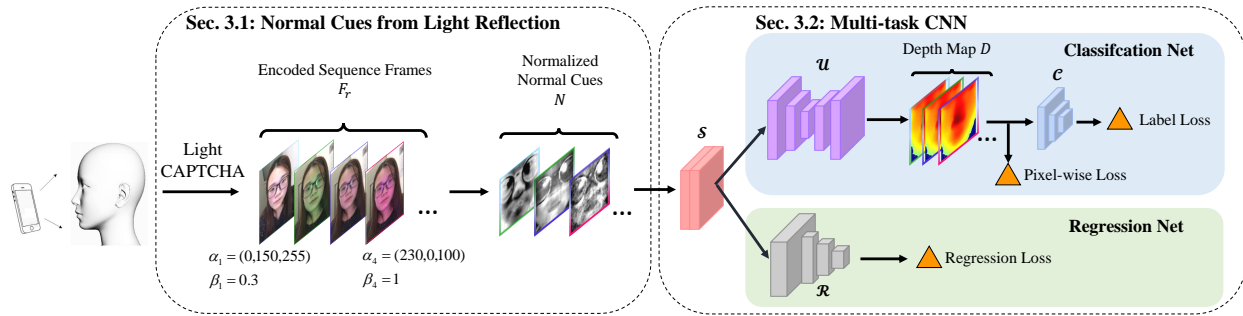


Figure 2: Overview of Aurora Guard. From facial reflection frames encoded by casted light CAPTCHA, we estimate the normal cues. In the classification branch, we recover the depth maps from the normal cues, and then perform depth-based liveness classification. In the regression branch, we obtain the estimated light CAPTCHA.

Moreover, since the imaging quality (resolution, device) and the types of Presentation Attack Instruments (PAI) are essential to evaluate performance in practical remote face authentication, we further build a dataset containing videos of facial reflection frames collected by our system, which is the most *comprehensive* and *largest* one in both aspects compared with other public datasets.

To sum up, the main contributions of this work include:

- A simple, fast yet effective face anti-spoofing method is proposed, which is practical in real scenarios *without* the requirement on specific hardware design.
- A *cost-free* depth recover net is proposed to estimate the facial depth maps via the *normal cues* extracted from the reflection frames for liveness classification.
- A novel *light CAPTCHA checking mechanism* is proposed to significantly improve the security against the attacks, especially the modality spoofing.
- A dataset containing comprehensive spoof attacks on various imaging qualities and mobile ends is built.

2 Related Work

Local Texture based Methods The majority of common presentation attacks are the recaptured images shown on printed photo and screens, in which the textures are different from the original images and can be leveraged to counter face spoofing. For example, Wen *et al.* [2015] adopted image distortion information as countermeasure against spoofing. Li *et al.* [2017] proposed Deep Local Binary Pattern (LBP) to extract LBP descriptors on convolutional feature map extracted by CNN. Boulkenafet *et al.* [2017] converted the face image from RGB color space to HSV-YCbCr space and extracted channel-wise SURF features Bay *et al.* [2006] to classify liveness result. However, since the above methods operate on 2D images, they still suffer from poor generalization ability to unseen attacks and complex lighting conditions, especially when RGB sensors have low resolution or quality. In contrast, our method exploits 3D information (*e.g.*, depth) via the reflection increments from RGB images, which makes our method more robust and accurate to various attacks.

Depth Sensor based Methods It is well known that the 3D facial cues can be used to defeat 2D presentation attacks. For example, Wang *et al.* [2017] directly exploit depth sensors such as Kinect to recover depth map and evaluate the anti-

spoofing effectiveness combined with texture features. Xie *et al.* [2017] introduced a light field camera to extract depth information from multiple refocused images took in one snapshot. Moreover, iPhone X incorporates a structured-light sensor to recover accurate facial depth map, which obtains impressive anti-spoofing performance. However, although iPhone X achieves high accuracy, there are two practical problems. First, it uses an *expensive* 3D camera for accurate depth. Second, its implementation details are missing. In contrast, our method is not only hardware-free that has competitive results against 3D hardware via a *cost-free* depth recover net, but also easy to follow for *re-implementation*.

Depth Estimated from Single Image Wang *et al.* [2013] firstly attempted to recover a sparse 3D facial structure from RGB image for face anti-spoofing. Atoum *et al.* [2017] proposed a two-stream depth-based CNN to estimate both texture and depth. Recently, Liu *et al.* [2018] fused multiple sequential depth predictions to regress to a temporal rPPG signal for liveness classification. However, 3D reconstruction from a single image is still highly under-constrained, since these methods suffer from missing solid 3D information clue. As a result, their anti-spoofing classifiers are hard to generalize to unseen spoof attacks, and is also sensitive against the quality of RGB camera. To address the inaccurate depth issue, our method first obtains normal cues based on the light reflection, which better removes the effects of albedo and illuminance. Then we train a compact encoder-decoder network to accurately recover the depth map.

Lambertian Reflection based Methods Tan *et al.* [2010] firstly pointed out the importance of Lambertian modeling for face anti-spoofing, while only obtains rough approximations of illuminance and reflectance parts. Chan *et al.* [2018] also adopted Lambertian reflection model to extract simple statistics (*i.e.*, standard deviation and mean) as features, but achieves limited performance. Our method differs from the above methods in three key aspects: (1) We *actively* perform light reflection via an extra light source specified by random light parameter sequence, while the above methods do NOT. (2) We construct a regression branch to achieve the novel *light CAPTCHA* checking mechanism to make the system more robust, while the above methods again lack such scheme. (3) We incorporate deep networks to learn powerful features, while the above methods use simple handcrafted features.

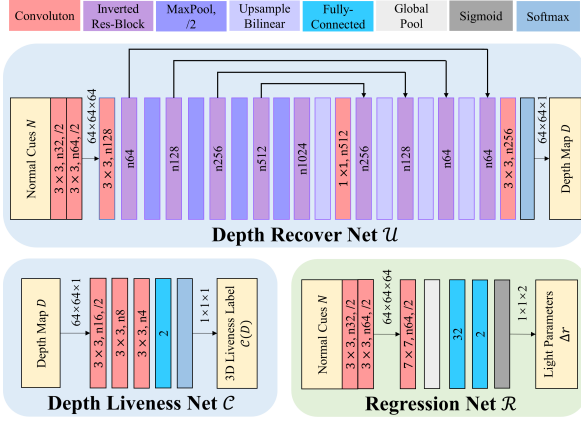


Figure 3: The architecture details of the proposed multi-task CNN. Here n denotes the number of output feature maps.

3 The Proposed Method

Fig. 2 illustrates the entire process of our method. Specifically, we first set a smart phone (or any other devices) with front camera and light source (*e.g.*, the screen) in front of the subject. Then, a random parameter sequence (*i.e.*, light CAPTCHA) of light hues and intensities is generated, *i.e.*, $r = \{(\alpha_i, \beta_i)\}_{i=1}^n$ given n frames. We manipulate the screen to cast dynamic light specified by the light CAPTCHA r . After the reflection frames F_r are captured, we sequentially estimate the normal cues N , which are the input of a multi-task CNN to predict liveness label and regress the estimated light CAPTCHA \hat{r} . The final judgement is been made from both of the predicted label and the matching result between \hat{r} and r .

3.1 Normal Cues from Light Reflection

Given the facial reflection frames $\{F_{r_i}\}_{i=1}^n$, we extract normal cues by estimating the reflection increments on subject’s face. Since objects with rough surfaces are diffuse reflectors (*e.g.* human face), light casted onto surface point is scattered and reflected, and then perceived as the final imaging in the camera. Given images containing reflection on the object surface, we measure the magnitude variations among different images, under the assumption of Lambertian reflection model and weak perspective camera projection.

Lambert’s Law regards the reflected part to be equal on all directions on the diffuse surface. In other words, for any pixel point \mathbf{p} of the camera image under specific casting light L_r , its intensity $F_r(\mathbf{p})$ is formulated as:

$$F_r(\mathbf{p}) = \rho_p(k_a + k_r \mathbf{l} \cdot \mathbf{n}_p), \quad (1)$$

where k_a is the ambient weight, k_r is the diffuse weight, \mathbf{l} is the light source direction, ρ_p is the albedo and \mathbf{n}_p is the point normal. When light changes suddenly, k_a and \mathbf{l} (position of the screen) are not supposed to change temporally and can be regarded as constants. We adopt affine transformation to align \mathbf{p}' and \mathbf{p} between image pairs, with transformation matrix estimated from the facial landmarks detected by PRNet Feng *et al.* [2018]. Then in another image under casting light $L_{r'}$, the intensity of the registered pixel \mathbf{p}' is:

$$F_{r'}(\mathbf{p}) = F_{r'}(\mathbf{p}') = \rho_{p'}(k_a + k_{r'} \mathbf{l} \cdot \mathbf{n}_{p'}). \quad (2)$$

We then attain the scalar product $N_{\Delta r}(\mathbf{p})$ on each point,

$$N_{\Delta r}(\mathbf{p}) = \mathbf{l} \cdot \mathbf{n}_p = \frac{F_r(\mathbf{p}) - F_{r'}(\mathbf{p})}{k_r - k_{r'}}, \quad (3)$$

where the scalar map arranged by $N_{\Delta r}(\mathbf{p})$ is the *normal cue*.

3.2 Multi-task CNN

After obtaining the normal cues, we adopt a multi-task CNN that has two branches to achieve liveness classification and light CAPTCHA regression, respectively. It should be noted that our multi-task structure is *task-driven*, which enables double checking mechanism to improve the robustness on modality spoofing in practical scenarios.

Liveness Classification. Depending on the lighting environment, the normal cues extracted from facial reflection frames may be rough and noisy. To efficiently obtain accurate depth information from the normal cues, we adopt an encoder-decoder network, which balances the performance and speed. The network architecture is inspired by Chen *et al.* [2018]; Ronneberger *et al.* [2015], in which we use the inverted residual block Sandler *et al.* [2018]. The recovered depth map is then sent to a simple classification structure to distinguish the real 3D face from those 2D presentation attacks. The detailed structure is shown in Fig. 3.

After obtaining m frames of normal cues N_1, N_2, \dots, N_m of one video, the classifier has the following loss function:

$$\begin{aligned} \mathcal{L}_{cls} = & \frac{1}{m} \sum_{i=1}^m \left\{ - (1 - \lambda_{depth})(c_i \log(\mathcal{C}(\mathcal{U}(\mathcal{S}(N_i)))) \right. \\ & + (1 - c_i) \log(1 - \mathcal{C}(\mathcal{U}(\mathcal{S}(N_i)))) \\ & \left. + \lambda_{depth} \sum_{\mathbf{p} \in \mathbb{Z}^2} -k \log(e^{d_k(\mathbf{p})} / (\sum_{k'=1}^{256} e^{d_{k'}(\mathbf{p})})) \right\}, \end{aligned} \quad (4)$$

where \mathcal{S} denotes stem operation that contains two convolutional layers, \mathcal{C} denotes the depth liveness prediction net, \mathcal{U} denotes the depth recover net, c_i is the liveness label of the i -th normal cue, λ_{depth} is the weight of the depth estimation loss. In depth recovering part, we adopt 2D pixel-wise soft-max over the predicted depth map combined with the cross-entropy loss function, where $k : \Omega \rightarrow 1, \dots, 256$ is the ground truth depth label, $d_k(\mathbf{p})$ is the feature map activation on channel k at the pixel position \mathbf{p} , while the feature map activation $\mathcal{U}(N_i)$ is the output of the depth recover net.

Light Parameter Regression. We reinforce the security of our method against *modality spoofing*, which is further discussed in Sec. 4.2, by customizing the casted light CAPTCHA and exploit a regression branch to decode it back for double checking automatically.

By feeding the same normal cues as the classification branch, the regression net has the loss function \mathcal{L}_{reg} as:

$$\mathcal{L}_{reg} = \frac{1}{m} \sum_{i=1}^m \{ \|\mathcal{R}(\mathcal{S}(N_i)) - \Delta r_i\|^2 \}, \quad (5)$$

where \mathcal{R} denotes the regression net, Δr_i is the ground truth light parameter residual of reflection frames F_{r_i} and $F_{r_{i-1}}$.

Supposing there are V videos in the training set, the entire loss function of our multi-task CNN is formulated as:

$$\mathcal{L}(\Theta) = \arg \min_{\Theta} \frac{1}{2V} \sum_{v=1}^V \{ \mathcal{L}_{cls}^v + \lambda_{reg} \mathcal{L}_{reg}^v \}, \quad (6)$$

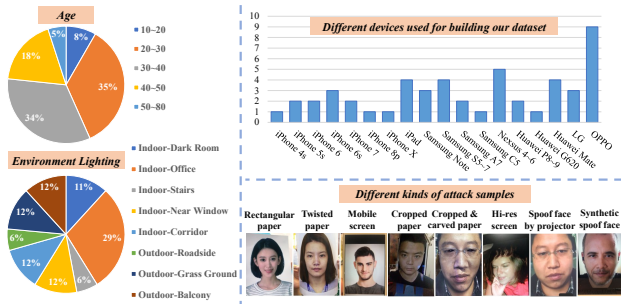


Figure 4: Statistics and attack samples of our dataset.

where Θ denotes the parameter set, λ_{reg} is the weight of CAPTCHA regression loss. In practice, we set the light CAPTCHA sequence to be composed by 4 types of light in random order, which balances the robustness of CAPTCHA checking and time complexity. We set the rate of light changing identical to the frame rate, thus the frames hold different light reflection. The length of F , r equals to $m+1$. The Signal-to-Noise Ratio (SNR) is adopted to check if the estimated light parameter sequence matches the ground truth sequence.

3.3 Dataset Collection

As claimed in Sec. 1, various imaging qualities and the types of PAIs are very important for practical remote face authentication. To address this need, we collect a new dataset, in which each data sample is obtained by casting dynamic light sequence onto the subject, and then record the 30-fps videos. Some statistics of the subjects are shown in Fig. 4. Note that we mainly collect 2D attacks, the main target in most prior anti-spoofing methods Atoum *et al.* [2017]; Liu *et al.* [2018], rather than 3D ones because the cost to produce and conduct 3D attacks in real scenarios is much higher than 2D attacks.

Compared to the previous public datasets Chingovska *et al.* [2012]; Liu *et al.* [2018]; Zhang *et al.* [2012], our dataset has three advantages: 1) Our dataset is the *largest* one that includes 12,000 live and spoof videos, with average duration to be 3s, collected from 200 subjects, compared to 4,620 videos from 165 subjects in Liu *et al.* [2018]. 2) Our dataset uses the *most extensive* devices (*i.e.*, 50 in ours vs. 4 in Liu *et al.* [2018]) to obtain good simulation of real-world mobile verification scenarios. 3) Our dataset contains the *most comprehensive* attacks that include various print, replay, modality and another spoof face by light projector (see Fig. 4).

We divide samples into 3 parts through the spoof types: paper attack, screen attack and other complex attacks consisting of cropped paper photos, projection attacks, *etc.* In each part, the data is further divided into train set, develop set and test set, as shown in Tab. 1. Moreover, the amounts of live data and spoof data stay equal in our dataset. The live data is collected under multiple variations including interference illumination on face, noisy imaging quality and different poses. The spoof data are collected through abundant PAIs.

4 Experiments

4.1 Implementation Details

Model Training We use Pytorch to implement our method and initialize all convolutional and fully-connected layers with

Table 1: Generalization experiment protocol. The train, development and test set are divided into 3:1:1 within the samples in each part.

Part	Type	Samples	Collection
Part 1	Paper Attack	2000	Phone No. 1~17
	Live Person	2000	Subject No.1~70
Part 2	Screen Attack	2200	Phone No. 18~34
	Live Person	2000	Subject No.71~140
Part 3	Complex Attack	1800	Phone No. 35~50
	Live Person	2000	Subject No.141~200

Table 2: Comparisons of EER from development set and $HTER$ from testing set in our dataset.

λ_{depth}	0.0	0.2	0.4	0.5
EER (%)	4.79 ± 0.41	2.31 ± 0.23	$1.58 \pm \mathbf{0.19}$	$\mathbf{1.48} \pm 0.21$
$HTER$ (%)	7.20 ± 0.77	3.53 ± 0.43	$2.21 \pm \mathbf{0.31}$	$\mathbf{2.09} \pm 0.33$

Table 3: Quantitative evaluation on modality spoofing.

	Video 1	Video 2	Video 3	Video 4	Video 5
FAR	2/3000	0/3000	0/3000	1/3000	0/3000
	0.06%	0.00%	0.00%	0.03%	0.00%

normal weight distribution He *et al.* [2015]. For optimization solver, we adopt RMSprop Graves [2013] during training process. Training our network roughly takes 5 hours using a single NVIDIA Tesla P100 GPU and iterates for ~ 300 epochs.

Evaluation Criteria We use common criteria to evaluate the anti-spoofing performance, including False Rejection Rate (FRR), False Acceptance Rate (FAR) and Half Total Error Rate ($HTER$), which depends on the threshold value τ_{cls} . To be specific, FRR and FAR are monotonic increasing and decreasing functions of τ_{cls} , respectively. A more strict classification criterion corresponds to a larger threshold of τ_{cls} , which means spoof faces are less likely to be misclassified. For certain data set \mathbb{T} and τ_{cls} , $HTER$ is defined by

$$HTER(\tau_{cls}, \mathbb{T}) = \frac{FRR(\tau_{cls}, \mathbb{T}) + FAR(\tau_{cls}, \mathbb{T})}{2} \in (0, 1). \quad (7)$$

Lower $HTER$ means better average performance on liveness classification, and $HTER$ reaches its minimum when $FAR=FRR$, which is defined as Equal Error Rate (EER).

4.2 Ablation Study

Effectiveness of Depth Supervision First, we conduct experiments to demonstrate the effects of the depth supervision. To be specific, we monotonically increase the weight of depth loss λ_{depth} in Eq. 4 and train multiple models, respectively. Under each λ_{depth} , we train 10 different models, and then evaluate the mean and standard variance of EER and $HTER$, as shown in Tab. 2. When $\lambda_{depth}=0$, the normal cues are directly used for liveness classification, which achieves the worst results. As we increase the λ_{depth} to give more importance on the auxiliary depth supervision, the performance improves gradually, which verifies its effectiveness to help denoise the normal cues and enhance the 3D information.

Light CAPTCHA Regression Branch Although our system can well handle most of the normal 2D presentation attacks via depth information, it may still suffer from one special spoofing attack named *modality spoofing*, which directly forges the desired reflection patterns. Specifically, modality spoofing will fail our classification net when meeting 2 requirement: 1) The formerly captured raw video consists of facial

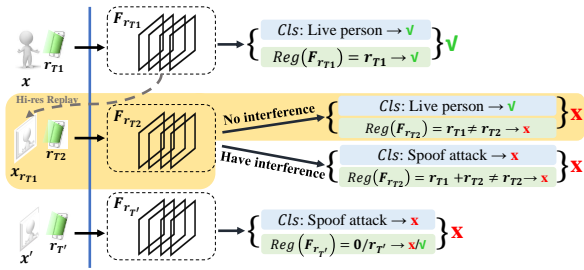


Figure 5: Illustration on our double checking mechanism. Cls , Reg are the classification net and regression net, respectively. 1) The first row handles live person. 2) The highlighted yellow part in the second row represents *modality spoofing* (i.e., $x_{r_{T1}}$), which replays the formerly captured Hi-res video frames $F_{r_{T1}}$ that contains true facial reflection, which fools the Cls but can be defended by the light CAPTCHA checking scheme in Reg . 3) No interference indicates the reflection effect caused by r_{T2} is **blocked**, thus $F_{r_{T2}}$ shares similar facial reflection with $F_{r_{T1}}$ and can pass the Cls . 4) The bottom row indicates the conventional 2D spoofing case.

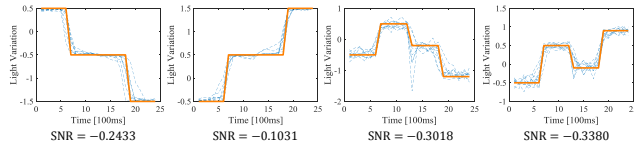


Figure 6: Illustration on estimated light CAPTCHA. Each figure shows 10 estimated curves obtained by our regression branch (blue dotted) from different subjects and scenes compared to the ground truth (orange solid), where the x-axis and y-axis denote the time and temporal variation of light hue α respectively.

Table 4: Comparison of EER from development set and $HTER$ from test set in our data set.

Method	EER (%)	$HTER$ (%)
SURF Boulkenafet <i>et al.</i> [2017]	4.72	14.65
Deep LBP Li <i>et al.</i> [2017]	5.61	8.83
FASNet Lucena <i>et al.</i> [2017]	5.67	8.60
Auxiliary Depth CNN Liu <i>et al.</i> [2018]	2.55	5.36
Ours	1.24	1.91

reflection frames, that contains the true reflection patterns, is leaked and replayed by Hi-res screen. 2) Within capture process of attack trial, the casted light doesn't interfere with the original facial reflection in video frames. Fig. 5 illustrates the principle of our light CAPTCHA against the modality spoofing. We further conduct experiments to prove the effectiveness of our light CAPTCHA checking mechanism in Fig. 6. The $|SNR|$ results of our regression branch are all below 0.35 and close with the ground truth CAPTCHA, which demonstrates its ability to distinguish 4 types of casting light.

Next, we quantitatively verify the effectiveness of our method against the modality spoofing attacks. We set the light CAPTCHA formed as the compositions of 4 types of casting light in a random order for every checking trial. To perform modality spoofing, we record videos consisting the same 4 types of true facial reflection (i.e., $F_{r_{T1}}$ in Fig. 5), and repeatedly replay the video for 3,000 times. In other words, the fixed video loop must match the randomly generated CAPTCHA to bypass our system. The experiment results in Tab. 3 show that the light CAPTCHA checking mechanism highly improves the security on modality spoofing.

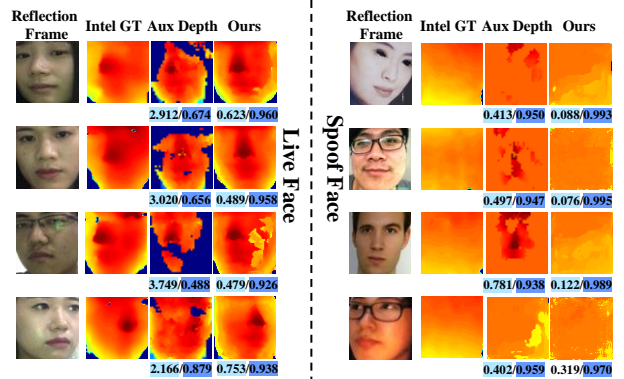


Figure 7: Comparisons on depth recovery. We take the depth data from Intel 3D camera as the ground truth. Results are computed using the depth metrics from Godard *et al.* [2017]. The light blue $RMSE(\log)$ measures error in depth values from the ground truth (Lower is better). And the dark blue $\delta < 1.25$ measures error in the percentage of depths that are within threshold from the correct value (Higher is better). Note that Aux Depth Liu *et al.* [2018] recovers depth map from single RGB image, while ours recovers from reflection frames which contain solid depth clues. The better recovered depth enables our method to accurately classify liveness, without additional texture or rPPG supervision.

4.3 Comparison to State-of-the-Art Methods

Depth Map Estimation Next, we conduct comparisons on depth recovery against the recent state-of-the-art method Liu *et al.* [2018], as shown in Fig. 7. We see that our method can recover more accurate depth map on various aspects, such as pose, facial contour and organ details, which demonstrate the effects to recover depth from solid depth clue instead of RGB texture. It should also be noted that our method achieves comparable results to the Intel 3D sensor that can absolutely detect 2D presentation attacks without failure cases.

Face Anti-Spoofing Here, we conduct comparisons on anti-spoofing, in which our method and several state-of-the-art methods are trained on our dataset (i.e., all the 3 training sets in each part), and then tested on public and our datasets, respectively. After training, we determine the threshold τ_{cls} via the EER on the develop set and evaluate the $HTER$ on the test set. First, we conduct test on our dataset. Tab. 4 shows that our method significantly outperforms the prior methods, where Aux Depth Liu *et al.* [2018] ranks 2nd, while the conventional texture based methods Boulkenafet *et al.* [2017]; Li *et al.* [2017] achieve relatively lower performance.

Next, we conduct tests on two public datasets: Replay-Attack Chingovska *et al.* [2012] and CASIA Zhang *et al.* [2012]. To better show the effectiveness and generalization of our method, *NO* additional fine-tuning is performed. Since our method requires casting extra light onto the subjects, the only way to test the live subjects is to let the real person involved in the public dataset to be presented, which is impossible and unable us to measure FRR on public dataset. For the spoof samples in these two public datasets, we print or broadcast the videos to act as the negative subjects and evaluate the FAR of various methods in Tab. 5. The results again demonstrate the effectiveness and generalization of our method compared to the state-of-the-art methods.

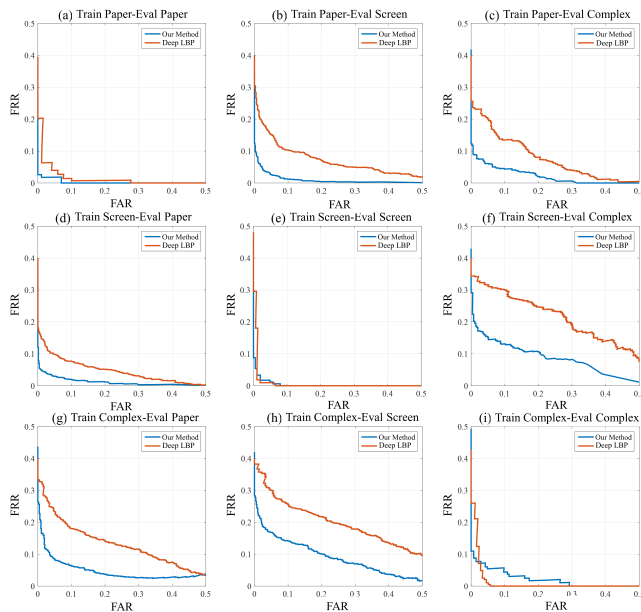


Figure 8: Generalization experiments with training and testing pairwise on every pair of sub-dataset combination.

Table 5: FAR indicator cross-tested on public dataset. Here to mention we use the same model trained from our data set without finetuning and same τ_{cls} to evaluate FAR on public dataset.

Method	Replay-Attack	CASIA
	$FAR(\%)$	$FAR(\%)$
Color texture Boulkenafet <i>et al.</i> [2015]	0.40	6.20
Fine-tuned VGG-face Li <i>et al.</i> [2016]	8.40	5.20
DPCNN Li <i>et al.</i> [2016]	2.90	4.50
SURF Boulkenafet <i>et al.</i> [2017]	0.10	2.80
Deep LBP Li <i>et al.</i> [2017]	0.10	2.30
Patch-Depth CNNs Atoum <i>et al.</i> [2017]	0.79	2.67
Ours	0.02	0.75

Model Generalization Robust generalization ability is a key characteristic for face anti-spoofing in real scenarios. Here, we conduct generalization comparisons with a state-of-the-art local texture based method Li *et al.* [2017], including live subject identity, device sensor interoperability and types of presentation attack. Specifically, we train both models from training set of each part in our dataset, and evaluate the performance in all three test sets respectively. Each model only learns one type of spoof attack with partial subject identities as well as device sensors, and the results are shown in Fig. 8. We can conclude that: 1) Curves (a),(e),(i) show that both models can achieve ideal FRR and FAR when training and evaluating are performed on the same attack. 2) Curves (b),(d) show that when testing on unseen attacks, the EER of Li *et al.* [2017] degrades to ~ 0.10 while our method is still below 0.04 with degradation of only ~ 0.01 . 3) Harder negatives from complex dataset lead to worse performance, where the EER of Li *et al.* [2017] in (i) rises from 0.03 to 0.22 in (h), while our method only goes up to 0.13. 4) In the other cases, our method retains half of the degradation on FAR and FRR , which demonstrates its robust generalization ability.

Running Time Comparison We compare cross-platform inference time with several SOTA methods. We deploy and

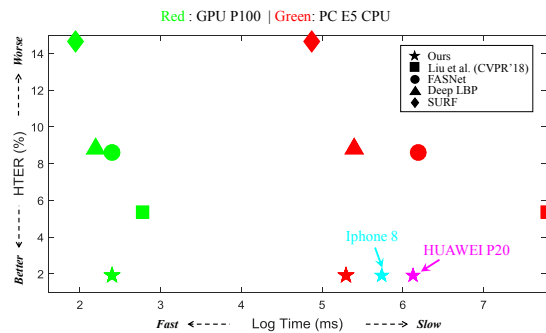


Figure 9: Time Comparison between several SOTA methods and ours in the aspects of effectiveness and cross-platform efficiency.

Table 6: FAR comparisons with SL3D. For each type of spoofing, we attack the system 100 times and count the passing cases.

Spoofing Type	SL3D	Ours-AG
Paper Photo (rect)	0/100	0/100
Paper Photo (crop,twist)	1/100	0/100
Paper Photo (crop,carve)	1/100	1/100
Screen Video (iPad)	0/100	0/100
Projector Spoof	0/100	0/100
$FAR(\%)$	0.40	0.20

compare on 3 common platform architectures: GPU for cloud server, CPU (x86) for some embedded chips and CPU (arm) for smart phones, as shown in Fig. 9. As we can see, our efficiency on mobile platform still meets the application requirement and even outperforms some methods on CPU (x86). The results indicate that our method achieves real-time efficiency and is portable for cross-platform computation requirements along with state-of-the-art anti-spoofing performance.

4.4 Comparison to Hardware-based Method

Finally, we compare our method with Structured-Light 3D (SL3D), which relies on the hardware that is embedded with structured-light 3D reconstruction algorithm. To be specific, we use an Intel[®] RealSense SR300 3D camera to obtain the facial depth map and adopt the same CNN classifier as in our multi-task network for SL3D. In contrast, our method only utilizes the ordinary RGB camera *without* specific hardware design. To comprehensively compare our method with SL3D, we only select and perform the hardest presentation attacks that could cause failure cases of 2D texture based methods. The results in Tab. 6 indicate that our method can achieve comparable anti-spoofing performance compared to SL3D.

5 Conclusion

In this paper, an effective facial anti-spoofing method named Aurora Guard is proposed, which holds real-time cross-platform applicability. The key novelty of our method is to leverage two kinds of auxiliary information, the depth map and the light CAPTCHA based on light reflection, which significantly improve the accuracy and reliability of anti-spoofing system against unlimited 2D presentation attacks. Extensive experiments on public benchmark and our dataset show that AG is superior to the state of the art methods.

References

- Yousef Atoum, Yaojie Liu, Amin Jourabloo, and Xiaoming Liu. Face anti-spoofing using patch and depth-based cnns. In *IEEE International Joint Conference on Biometrics (IJCB)*, 2017.
- Herbert Bay, Tinne Tuytelaars, and Luc Van Gool. Surf: Speeded up robust features. In *Proceedings of European Conference on Computer Vision (ECCV)*, 2006.
- Zinelabidine Boulkenafet, Jukka Komulainen, and Abdenour Hadid. Face anti-spoofing based on color texture analysis. In *IEEE International Conference on Image Processing (ICIP)*, 2015.
- Zinelabidine Boulkenafet, Jukka Komulainen, and Abdenour Hadid. Face antispoofing using speeded-up robust features and fisher vector encoding. *IEEE Signal Processing Letters*, 24(2):141–145, 2017.
- Patrick PK Chan, Weiwen Liu, Danni Chen, Daniel S Yeung, Fei Zhang, Xizhao Wang, and Chien-Chang Hsu. Face liveness detection using a flash against 2d spoofing attack. *IEEE Transactions on Information Forensics and Security*, 13(2):521–534, 2018.
- Yu Chen, Ying Tai, Xiaoming Liu, Chunhua Shen, and Jian Yang. Fsrnet: End-to-end learning face super-resolution with facial priors. In *Proceedings of the IEEE Conference on Computer Vision and Pattern Recognition (CVPR)*, 2018.
- Ivana Chingovska, André Anjos, and Sébastien Marcel. On the effectiveness of local binary patterns in face anti-spoofing. In *Proceedings of the International Conference of Biometrics Special Interest Group (BIOSIG)*, 2012.
- Yao Feng, Fan Wu, Xiaohu Shao, Yanfeng Wang, and Xi Zhou. Joint 3d face reconstruction and dense alignment with position map regression network. In *Proceedings of European Conference on Computer Vision (ECCV)*, 2018.
- Clément Godard, Oisín Mac Aodha, and Gabriel J Brostow. Unsupervised monocular depth estimation with left-right consistency. In *Proceedings of IEEE Conference on Computer Vision and Pattern Recognition (CVPR)*, 2017.
- Alex Graves. Generating sequences with recurrent neural networks. *arXiv preprint arXiv:1308.0850*, 2013.
- Kaiming He, Xiangyu Zhang, Shaoqing Ren, and Jian Sun. Delving deep into rectifiers: Surpassing human-level performance on imagenet classification. In *Proceedings of the IEEE International Conference on Computer Vision (ICCV)*, 2015.
- Lei Li, Xiaoyi Feng, Zinelabidine Boulkenafet, Zhaoqiang Xia, Mingming Li, and Abdenour Hadid. An original face anti-spoofing approach using partial convolutional neural network. In *International Conference on Image Processing Theory Tools and Applications (IPTA)*, 2016.
- Lei Li, Xiaoyi Feng, Xiaoyue Jiang, Zhaoqiang Xia, and Abdenour Hadid. Face anti-spoofing via deep local binary patterns. In *IEEE International Conference on Image Processing (ICIP)*, 2017.
- Yaojie Liu, Amin Jourabloo, and Xiaoming Liu. Learning deep models for face anti-spoofing: Binary or auxiliary supervision. In *Proceedings of the IEEE Conference on Computer Vision and Pattern Recognition (CVPR)*, 2018.
- Oeslle Lucena, Amadeu Junior, Vitor Moia, Roberto Souza, Eduardo Valle, and Roberto Lotufo. Transfer learning using convolutional neural networks for face anti-spoofing. In *Proceedings of International Conference Image Analysis and Recognition (ICIAR)*, 2017.
- Olaf Ronneberger, Philipp Fischer, and Thomas Brox. U-net: Convolutional networks for biomedical image segmentation. In *International Conference on Medical Image Computing and Computer-Assisted Intervention (MICCAI)*, 2015.
- Mark Sandler, Andrew Howard, Menglong Zhu, Andrey Zhmoginov, and Liang-Chieh Chen. Mobilenetv2: Inverted residuals and linear bottlenecks. In *Proceedings of the IEEE Conference on Computer Vision and Pattern Recognition (CVPR)*, 2018.
- Xiaoyang Tan, Yi Li, Jun Liu, and Lin Jiang. Face liveness detection from a single image with sparse low rank bilinear discriminative model. In *Proceedings of European Conference on Computer Vision (ECCV)*, 2010.
- Tao Wang, Jianwei Yang, Zhen Lei, Shengcai Liao, and Stan Z Li. Face liveness detection using 3d structure recovered from a single camera. In *Proceedings of International Conference on Biometrics (ICB)*, 2013.
- Yan Wang, Fudong Nian, Teng Li, Zhijun Meng, and Kongqiao Wang. Robust face anti-spoofing with depth information. *Journal of Visual Communication and Image Representation*, 49:332–337, 2017.
- Di Wen, Hu Han, and Anil K. Jain. Face spoof detection with image distortion analysis. *IEEE Transactions Information Forensics and Security*, 10(4):746–761, 2015.
- Xiaohua Xie, Yan Gao, Wei-Shi Zheng, Jianhuang Lai, and Junyong Zhu. One-snapshot face anti-spoofing using a light field camera. In *Proceedings of Chinese Conference on Biometric Recognition (CCBR)*, 2017.
- Dong Yi, Zhen Lei, Zhiwei Zhang, and Stan Z Li. Face anti-spoofing: Multi-spectral approach. In *Handbook of Biometric Anti-Spoofing*, pages 83–102. Springer, 2014.
- Z. Zhang, J. Yan, S. Liu, Z. Lei, D. Yi, and S. Z. Li. A face antispoofing database with diverse attack. In *Proceedings of International Conference on Biometrics (ICB)*, 2012.